Simulation Study of the Effect of the Chemical Heterogeneity of Activated Carbon on Water Adsorption

Miguel Jorge, Christian Schumacher, and Nigel A. Seaton*

School of Chemical Engineering, University of Edinburgh, King's Buildings, Mayfield Road, Edinburgh, EH9 3JL, UK

Received April 19, 2002. In Final Form: August 29, 2002

In this paper we present results from the molecular simulation of water adsorption in slit-shaped activated carbon pores. We calculate adsorption isotherms by grand canonical Monte Carlo (GCMC) simulation, Henry's constants by Monte Carlo integration, and vapor−liquid equilibrium data by the gauge-cell Monte Carlo method, to investigate the chemical heterogeneity of activated carbon adsorbents. Several types of polar oxygen-containing sites are placed on the surface of the carbon with different densities and local distributions, in order to determine the individual effects of each of these factors on the adsorption of water. Our results confirm the role of surface sites in the enhancement of water adsorption. Furthermore, we show that the local distribution of these sites has a strong effect on low-pressure adsorption, while the overall site density affects mainly the vapor−liquid phase transition. The type of oxygen-containing group is shown not to be of critical importance, since more complex groups can effectively be represented by simpler sites. This study forms the basis for the development of a model for activated carbon that is able to represent the chemical heterogeneity of this type of material.

Introduction

Activated carbons consist of a more or less irregular stacking of graphitic plates, the interstices of which constitute the pores.[1] This structural heterogeneity of an activated carbon adsorbent can be approximated by a distribution of slit-shaped pores. Such a model has been used successfully to describe the adsorption of essentially nonpolar species such as nitrogen or light hydrocarbons (see refs 2−6 and references therein). However, in the case of the adsorption of polar species, other characteristics of the adsorbent come into play. Depending on the nature of the precursor and on the activation process, oxygen-containing groups can be bound to the edges of the graphitic plates or to defect sites such as vacancies.[7] These groups are usually polar in nature and can interact with polar species, increasing the affinity of the carbon for these substances. Oxygen functional groups can be present in several forms, such as carboxyl, carbonyl, and hydroxyl, and these can combine to form more complex arrangements.[8] Several techniques, such as titration,[9,10] temperature programmed desorption,[11] Fourier transform Infrared spectroscopy,[11,12] and X-ray photoelectron spectroscopy[13] have been employed to determine the nature and concentration of these sites (for a review, see ref 8).

It has long been recognized from experiment that the presence of polar surface groups can dramatically affect the adsorption of polar species such as water.[14] Walker and Janov[15] correlated the amount of water adsorbed with the concentration of oxygen at the surface of nonporous carbon, while Dubinin[16] proposed a mechanism for water adsorption in activated carbon based on primary adsorption on surface oxides followed by clustering of water molecules and pore filling at higher pressures. It was suggested by Barton et al.[17] that the extent of adsorption is not dependent on the structure of the oxygenated groups but only on the concentration of oxygen at the surface. Several researchers[13,18−20] have shown that an increase in the amount of surface polarity, brought about by oxidation of the carbon, causes an increase in the low-pressure water adsorption and/or a shift of the inflection point of the adsorption isotherm to lower pressures. This suggests that polar sites have a strong effect on both physical adsorption of water vapor and on the phenomenon of capillary condensation. However, it is still impossible, from a purely experimental point of view, to selectively study the influence of the type, concentration, and location of these sites on adsorption, as well as separating these effects from other features of the adsorbent (such as the distribution of pore sizes and surface defects). Molecular simulation provides an excellent tool for this purpose.

There have been few molecular simulation studies of water adsorption in carbon pores. To our knowledge, the first authors to address this subject were Ulberg and Gubbins,[21] who published pure water adsorption isotherms in a slit-shaped graphitic pore, using a point charge

* Corresponding Author. E-mail: n.seaton@ed.ac.uk. Telphone: (+44) 131 650 4867. Fax: (+44) 131 650 6551.

(1) McEnaney, B. *Carbon* **1988**, *26*, 267.
(2) Seaton, N. A.; Walton, J. P. R. B.; Quirke, N. *Carbon* **1989**, *27*, 853.
(3) Davies, G. M.; Seaton, N. A. *Langmuir* **1999**, *15*, 6263.
(4) Qiao, S.; Wang, K.; Hu, X. *Langmuir* **2000,** *16*, 1292.
(5) Nguyen, C.; Do, D. D. *Langmuir* **2000**, *16*, 1319.
(6) Ravikovitch, P. I.; Vishnyakov, A.; Russo, R.; Neimark, A. V. *Langmuir* **2000**, *16*, 2311.
(7) Thomas, J. M. In *Chemistry and Physics of Carbon;* Walker, P. L., Jr., Ed., Marcel Dekker: New York, 1965; Vol. 1.
(8) Boehm, H. P. *Carbon* **1994**, *32*, 759.
(9) Boehm, H. P., 1966, In: Advances in Catalysis, Vol. 16, Academic Press: New York.
(10) Salame, I. I.; Bandosz, T. J. *Langmuir* **1999**, *15*, 587.
(11) Jia, Y. F.; Thomas, K. M. *Langmuir* **2000,** *16*, 1114.
(12) Meldrum, B. J.; Rochester, C. H. *J. Chem. Soc., Faraday Trans.* **1990**, *86*, 861.
(13) Kaneko, Y.; Ohbu, K.; Uekawa, N.; Fujie, K.; Kaneko, K. *Langmuir* **1995**, *11*, 708.
(14) Rouquerol, F.; Rouquerol, J.; Sing, K. *Adsorption by Powders and Porous Solids;* Academic Press: London, 1999.
(15) Walker, P. L.; Janov, J. J. *Colloid Interface Sci.* **1968**, *28*, 449.
(16) Dubinin, M. M. *Carbon* **1980**, *18*, 355.
(17) Barton, S. S.; Evans, M. J. B.; MacDonald, J. A. F. *Langmuir* **1994**, *10*, 4250.
(18) Rodriguez-Reinoso, F.; Molina-Sabio, M.; Muñecas, M. A. *J. Phys. Chem.* **1992**, *96*, 2707.
(19) Carrasco-Marín, F.; Mueden, A.; Centeno, T. A.; Stoeckli, F.; Moreno-Castilla, C. *J. Chem. Soc., Faraday Trans.* **1997**, *93*, 2211.
(20) Salame I. I.; Bandosz T. J., 1999, *Langmuir* **1999**, *15*, 587.
(21) Ulberg, D. E.; Gubbins, K. E. *Mol. Phys.* **1995,** *84*, 1139.

10.1021/la025846q CCC: $22.00
Published on Web 10/25/2002

model—TIP4P— to represent the water molecule. Their results demonstrated the importance of hydrogen bonding to the mechanism of adsorption. Maddox et al.[22]followed from their work to include polar carboxyl sites on the surface of the pore. They concluded that the presence of these sites significantly enhances the adsorption of water but also observed that isolated sites have a very small impact on water adsorption.

Müller and co-workers[23−25] developed a simplified model for water, replacing the charges by square-well sites that were able to mimic hydrogen bonds between molecules, so as to reduce the complexity of the calculation and the computer requirements. They have performed simulations of adsorption of pure water[23] and methane/water mixtures[24] on activated carbon. Their results agreed with the cooperative adsorption mechanism proposed by Dubinin.[16] These authors also observed that even at a high degree of pore filling some isolated sites remained unoccupied. Müller et al.[23] studied a series of surface site configurations with varying local site density (maintaining the overall site concentration constant) and concluded that sites that are closely placed exert a stronger influence on water adsorption. They suggested that the local placement of the sites dominates over the overall concentration in determining the adsorption behavior. McCallum et al.[25] analyzed the influence of site concentration on water adsorption isotherms and concluded that at a sufficiently high degree of activation, the pore filling mechanism becomes continuous, as opposed to discontinuous as in the case of graphite. They suggested the existence of a limiting site density above which a continuous pore filling will be observed.

The objective of this paper is to separately study the different factors associated with the presence of polar sites on the extent and mechanism of water adsorption. We present a detailed and systematic study of the effect of density, distribution, and type of oxygen-containing sites on water adsorption, by calculating adsorption isotherms, Henry's constants of adsorption, and phase equilibrium data using molecular simulation.

Potential Models

Water is represented by the SPC/E potential,[26] which consists of a Lennard-Jones (L-J) site and a negative charge at a location corresponding to the oxygen atom and two positive point charges located at the positions of the hydrogen atoms. All the parameters for this model were taken from Berendsen et al.[26] The pores are bounded by two parallel walls, each of which comprises an infinite number of layers of graphite. The graphite layers are composed of Lennard-Jones sites, but these are smeared out uniformly over each layer. The interaction between an adsorbate molecule and this smooth carbon surface is represented by the 10−4−3 potential of Steele.[27] We have studied three different types of polar surface sites: hydroxyl, carboxyl and carbonyl groups, represented schematically in Figure 1. A carboxyl site is constituted by three Lennard-Jones sites and five point charges, a hydroxyl site contains only one L-J site and three charges, and a carbonyl site is simply one L-J site and two point charges.

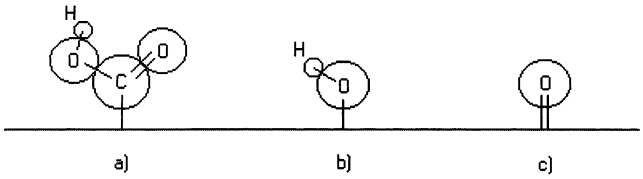

Figure 1. Schematic representation of the polar surface sites studied in this work: (a) a carboxyl group; (b) a hydroxyl group; (c) a carbonyl group.

Table 1. Potential Parameters for All Species Studied in This Work

	site	σ, nm	ϵ, J mol^{-1}	q/e
water	H	0.0	0.0	+0.4238
	O	0.3166	650.2	0.8476
graphite	C	0.340	232.8	0.0
Carbonyl	C[a]	0.0	0.0	+0.5
	O	0.296	879.6	0.5
hydroxyl	C[a]	0.0	0.0	+0.2
	O	0.307	650.2	0.64
	H	0.0	0.0	+0.44
carboxyl	C[a]	0.0	0.0	+0.08
	C	0.375	439.0	+0.55
	=O	0.296	878.8	0.5
	O	0.300	711.7	0.58
	H	0.0	0.0	+0.45

[a] Carbon atom in the graphite basal plane.

Table 2. Geometric Parameters for All Species Studied in This Work

	bond	length, nm	angle	amplitude, deg
water	OH	0.10	HOH	109.47
carbonyl	C[a]O	0.1233		
hydroxyl	C[a]O	0.1364	C[a]OH	110.5
	OH	0.096		
carboxyl	C[a]C	0.152	C[a]CO	111
	C=O	0.1214	OCO	123
	CO	0.1364	COH	107
	OH	0.097		

[a] Carbon atom in the graphite basal plane.

Parameters for hydroxyl groups were taken from the model of Mooney et al.[28] for phenol molecules. This model is thought to accurately represent OH groups bonded to aromatic rings. Since suitable models for carboxyl and carbonyl groups bonded to aromatic rings were not available in the literature, L-J parameters and point charges for these groups have been adopted from the OPLS potential models for acetic acid[29] and amino acids,[30] respectively. It should be noted here that the presence of an aromatic ring should have a stabilizing influence over the functional groups, causing their charges to be slightly reduced. Although this will be valid for both COOH and =O groups, we have kept the original parameters of the OPLS potential.

In Table 1, we show the potential parameters for water, graphite, and surface sites, while in Table 2 we present the corresponding geometric parameters. Cross-species Lennard-Jones parameters were calculated by using the Lorentz−Berthelot combining rules.

(22) Maddox, M.; Ulberg, D. E.; Gubbins, K. E. *Fluid Phase Equilib.* **1995**, *104*, 145.
(23) Müller, E. A.; Rull, L. F.; Vega, L. F.; Gubbins, K. E. *J. Phys. Chem.* **1996,** *100*, 1189.
(24) Müller, E. A.; Gubbins, K. E. *Carbon* **1998**, *36*, 1433.
(25) McCallum, C. L.; Bandosz, T. J.; McGrother, S. C.; Müller, E. A.; Gubbins, K. E. *Langmuir* **1999,** *15*, 533.
(26) Berendsen, H. J. C.; Grigera, J. R.; Straatsma, T. P. *J. Phys. Chem.* **1987**, *91*, 6269.
(27) Steele, W. A. The Interaction of Gases with Solid Surfaces; Pergamon Press: Oxford, 1974.
(28) Mooney, D. A.; Müller-Plathe, F.; Kremer, K. *Chem. Phys. Lett.* **1998**, *294*, 135.
(29) Briggs, J. M.; Nguyen, T. B.; Jorgensen, W. L. *J. Phys. Chem.* **1991**, *95*, 3315.
(30) Jorgensen, W. L.; Tirado-Rives, J. *J. Am. Chem. Soc.* **1988**, *110*, 1657.

Simulation Methods

Grand Canonical Monte Carlo Method. We have calculated adsorption isotherms using grand canonical Monte Carlo (GCMC) simulations, in which the temperature (T), volume (V), and chemical potential (μ) are kept constant. The algorithm for GCMC simulations is well-documented[31,32] and we have used the general methodology. The pressure (P) was calculated from the chemical potential by the Peng−Robinson equation of state[33] and all the simulations presented in this paper were performed in equilibrium with a bulk gas at 298 K. Each type of MC trial (creation, destruction, and displacement/rotation) was chosen randomly with the same probability. The number of equilibration steps in the simulations varied according to the operating conditions, but was never less than 5×10^6 and was as large as 10^7 for the highest densities. During the sampling period, typical configurations for each run were stored in files and then converted into images. To represent an essentially infinite slit-shaped pore, we have used a rectangular simulation cell, bound in the z direction by the pore walls and replicated in the x and y directions using periodic boundary conditions. The length of the simulation cell in both directions parallel to the walls was chosen to be 3 nm for all pore sizes, since this was shown to be large enough to avoid any finite size effects.[34] The potential between two point charges is long-ranged in nature and its calculation requires the use of special techniques. After comparing the performance of a number of these techniques for this type of application,[35] we have chosen a method proposed by Heyes and van Swol,[36] which performs a summation of the Coulomb potential over a small number of periodic boxes and then includes a correction term for the remaining boxes up to infinity. In a previous publication[35] we describe the efficient implementation of the GCMC algorithm for water adsorption studies in detail.

Henry's Constant by Monte Carlo Integration. The Henry's constant (H) is defined as

$$H = \lim_{P \to 0} \frac{\langle N \rangle}{VP} \tag{1}$$

where $\langle N \rangle$ is the average number of molecules in the pore. We have used a procedure proposed by Smit and Siepmann,[37] which relates the Henry's constant to the potential energy:

$$H = \frac{\left\langle \exp\left(-\frac{U}{k_B T}\right) \right\rangle}{k_B T} \tag{2}$$

where k_B is Boltzmann's constant. The Boltzmann factor, in angular brackets in this equation, is sampled by repeatedly inserting a water molecule at random locations in the pore and calculating the potential due to this insertion (U). In all our simulations this calculation was performed over at least 5×10^6 insertion steps, which produced an error of at most 2% in the Henry's constant.

To confirm that the value of the Henry's constant obtained by this method is accurate, we have compared it with the slope of an isotherm obtained by GCMC at very low pressures (Figure 2).

We can see that the slope calculated by Monte Carlo integration agrees well with the isotherm points, which shows the consistency of both methods. The values of Henry's constant obtained in this way describe adsorption in the low-pressure limit and provide us with a measure of the affinity of the pore for the adsorption of water. The higher the Henry's constant, the stronger the affinity of the pore toward water, i.e., the higher the hydrophilicity. In the remainder of this work, values of Henry's constant will be presented in reduced units ($H^* = Hk_BT$).

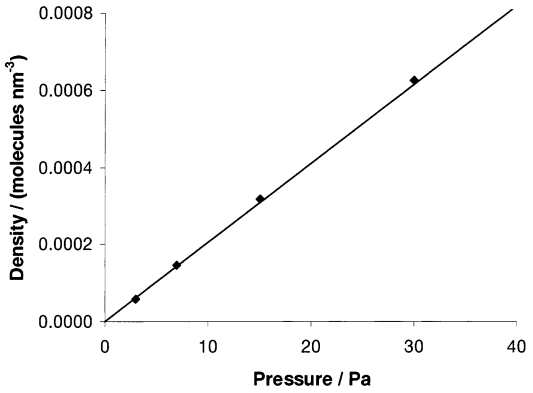

Figure 2. Comparison of Henry's constant calculated by Monte Carlo integration (line) with isotherm points from GCMC simulation (diamonds).

Gauge-Cell Method. Although the GCMC method is extremely useful for adsorption studies, it presents a disadvantage when the adsorbate is subcritical. In such a case, the point of equilibrium phase coexistence is, in practice, unattainable in a GCMC simulation. Instead, the isotherms show significant hysteresis between the adsorption and desorption branches.[34,38] Since in most cases of interest water adsorbed on activated carbon is under subcritical conditions, the need arises for a more complete treatment of the phase equilibrium. Therefore, we have performed simulations of water in activated carbon pores using the recently proposed gauge-cell Monte Carlo method, which is capable of calculating the correct value of the pressure at the equilibrium phase transition.

The gauge-cell method, proposed by Neimark and Vishnyakov,[39] is essentially a particular implementation of a pore-bulk Gibbs ensemble simulation.[40] The system consists of two separate simulation cells that are allowed to exchange molecules with one another. Both pore and bulk (gauge) cells have fixed volumes and are kept at the same constant temperature. By adjusting the total number of molecules in the system and the volume of the gauge cell, one can restrict the density fluctuations inside the pore. We are thus able to sample the complete continuous isotherm, including stable, metastable, and unstable branches. The pressure can be calculated from the density in the gauge cell by performing independent simulations in the gauge cell alone. At the bulk-gas conditions used in our simulations, the gauge cell contains an essentially ideal gas so the pressure and the density can simply be related by the ideal gas law.[34] Once the entire van der Waals loop has been obtained, it is possible to calculate the pressure at the equilibrium phase transition by employing Maxwell's rule of equal areas.[39]

The cell representing the pore is identical with that used in the GCMC simulations. The gauge cell was cubic and periodic boundary conditions were applied in all three directions. The method requires two different types of trial—particle displacement/rotation in each cell and particle exchange between both cells—and each of these was chosen randomly with equal probability. During each run, the system was allowed to equilibrate for at least 6×10^6 steps. Long-range interactions in the pore cell were handled by using the method of Heyes and van Swol,[36] while the standard three-dimensional Ewald sums[31] were employed in the gauge cell. Practical details regarding the implementation of this method have been given previously.[34]

Results and Discussion

Effect of Lateral Separation of Surface Sites. We have calculated H for a series of configurations where two carbonyl groups are placed on the same wall and

(31) Allen, M. P.; Tildesley, D. J. *Computer Simulation of Liquids;* Clarendon Press: Oxford, 1989.
(32) Frenkel, D.; Smit, B. *Understanding Molecular Simulation*; Academic Press: London, 1996.
(33) Sandler, S. I. *Chemical and Engineering Thermodynamics*; Wiley: New York, 1989.
(34) Jorge, M.; Seaton, N. A., submitted to *Mol. Phys.*
(35) Jorge, M.; Seaton, N. A. *Mol. Phys.* **2002,** *100*, 2017.
(36) Heyes, D. M.; van Swol, F. *J. Chem. Phys.* **1981**, *75*, 5051.
(37) Smit, B.; Siepmann, J. I. *J. Phys. Chem.* **1994**, *98*, 8442.
(38) Schoen, M.; Rhykerd, C. L.; Cushman, J. H.; Diestler, D. *J. Mol. Phys.* **1989**, *66*, 1171.
(39) Neimark, A. V.; Vishnyakov, A. *Phys. Rev. E* **2000**, *62*, 4611.
(40) Panagiotopoulos, A. Z. *Mol. Phys.* **1987**, *62*, 701.

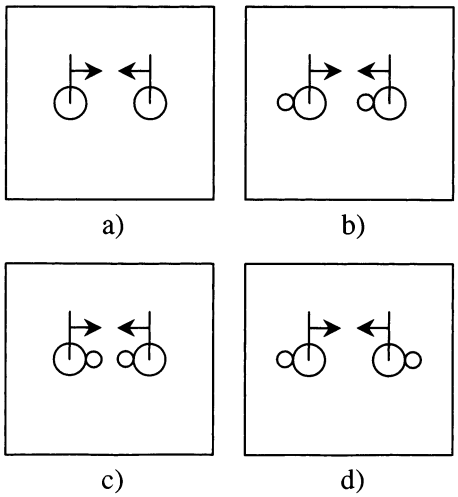

Figure 3. Configurations for the study of lateral separation between surface sites: (a) carbonyl sites; (b) codirectional hydroxyl sites; (c) converging hydroxyl sites; (d) opposing hydroxyl sites. The *x* direction is from left to right, the *y* direction is from bottom to top, and the *z* direction is outward from the page.

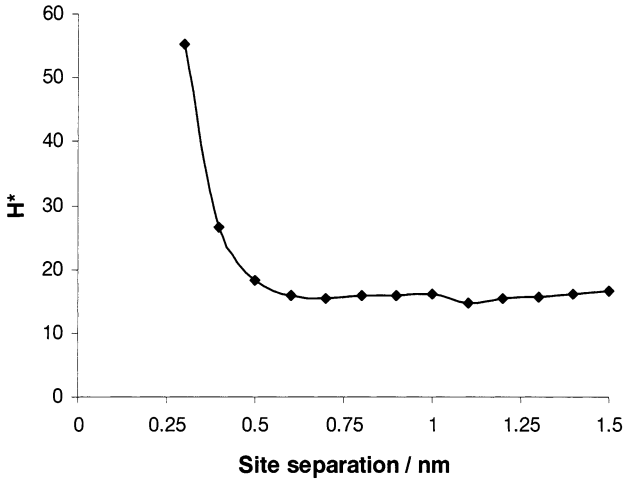

Figure 4. Henry's constant as a function of the separation distance between two carbonyl sites located on the same wall. The pore width is 0.95 nm. The line is a guide to the eye. Error bars are the size of the symbols used.

their relative separation along the *x* direction is changed (Figure 3a).

The maximum separation distance was set at half the box length (1.5 nm) and the minimum at approximately the Lennard-Jones diameter of the oxygen atom (0.3 nm). From the plot shown in Figure 4, we can see that adsorption is significantly enhanced when the distance between the two sites is less than 0.6 nm. Above this threshold, there is no noteworthy variation in Henry's constant, indicating that the carbonyl groups are essentially behaving as isolated sites.

The highest value of *H* occurs at a distance of 0.3 nm, which means that water is preferentially adsorbed near two carbonyl groups that are very close together. The reason for this is that in this case one water molecule can hydrogen bond with both surface sites at the same time, as seen in the snapshot in Figure 5a. This configuration is energetically very favorable, leading to a large Henry's constant.

When the sites are separated by at least 0.6 nm, the water molecule can no longer reach both sites at the same time, so it simply bonds to one of them (Figure 5b). After

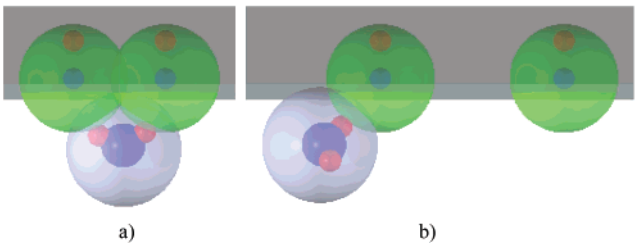

Figure 5. Snapshots of water adsorbing in a slit pore of width 0.95 nm with two carbonyl sites. Separation distances between sites are 0.3 (a) and 0.6 nm (b). The transparent spheres are the Lennard-Jones centers (green for surface sites and light blue for water), while the solid spheres represent point charges (blue for negative and red for positive).

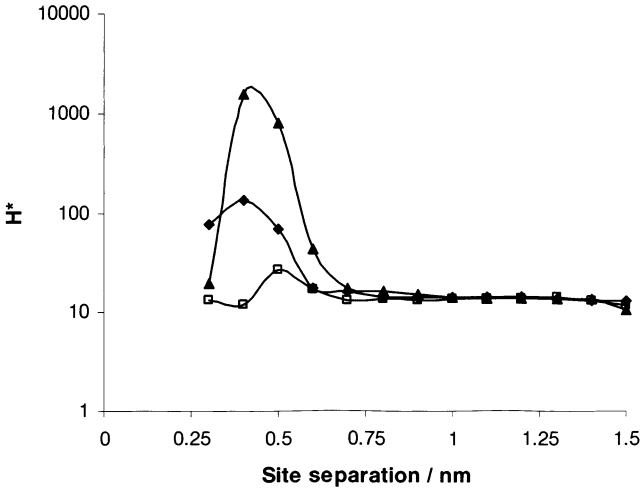

Figure 6. Henry's constant as a function of separation distance between two hydroxyl sites located on the same wall. The pore width is 0.95 nm. Diamonds are for opposing hydrogens, triangles are for converging hydrogens, and open squares are for codirectional hydrogens. Lines are a guide to the eye.

this point, the contribution of each surface site to the affinity of the pore for water adsorption is independent of their separation.

We have performed an analogous study involving hydroxyl groups, but in this case the orientation of the sites must be taken into consideration. We have therefore varied the distance between two OH groups on the same wall for three different orientations—in one case the hydrogens are pointing in the same direction (codirectional, Figure 3b), in another case they are pointing toward each other (converging, Figure 3c), and in the final case they point away from each other (opposing, Figure 3d). The results for the three orientations are plotted in Figure 6.

For the case of converging hydrogens, the maximum enhancement of adsorption happens when the sites are separated by 0.4−0.5 nm. At this distance, a water molecule can "fit" between the two sites in an extremely favorable configuration, with the electronegative oxygen atom located between the two hydrogens of the hydroxyl groups (Figure 7a). When the sites are too close together (0.3 nm), the water molecule starts to feel the repulsive forces between the negative oxygen atoms and this configuration becomes unfavorable. This behavior is quite distinct from that of carbonyl groups, because in the latter case the water molecules can form hydrogen bonds from every direction in the pore volume with no interference from opposite charges.

If we now look at the case of opposing hydrogens, again we see that the highest value of the Henry's constant occurs at a separation of 0.4 nm. This corresponds to a config-

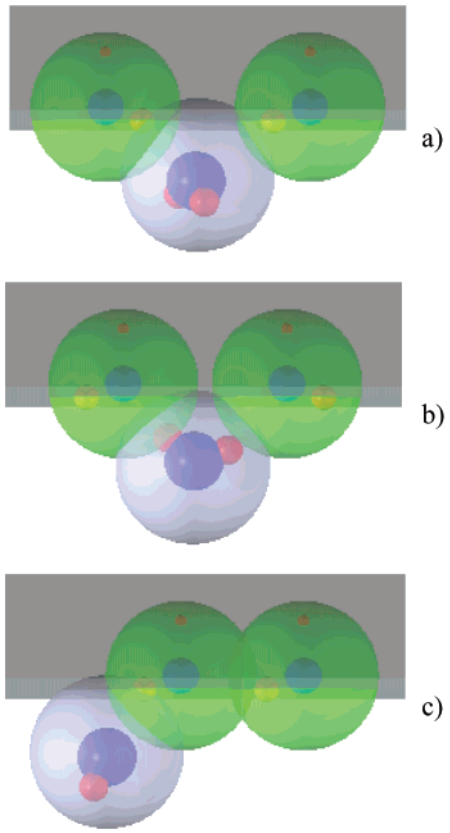

Figure 7. Snapshots of water adsorption in a slit pore of width 0.95 nm with two hydroxyl groups: (a) is for converging, (b) for opposing, and (c) for codirectional hydrogens. Color coding is the same as in Figure 5.

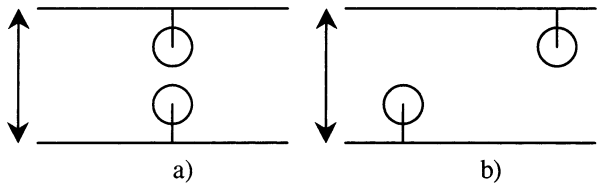

Figure 8. Configurations for the study of pore width variations with carbonyl sites: (a) directly above each other; (b) at maximum lateral distance.

uration in which the water molecule bonds to both sites simultaneously, this time with each hydrogen atom pointing toward one surface site (Figure 7b). Both the opposing and converging configurations cause an appreciable enhancement in adsorption of water when the sites are a suitable distance apart (the latter being slightly more favorable). However, in the codirectional configuration this enhancement is not so evident, due to a shielding effect of the oxygen charge. The negative charge of one site is "protected" by a positive hydrogen of the neighboring site, and vice-versa (Figure 7c). For this orientation, there is almost no change in H with the separation distance, since a water molecule can bond to only one of the sites. In general, regardless of the orientation, the sites behave as if they were isolated at distances above 0.7 nm (H is essentially constant above this value). This distance is larger than that corresponding to carbonyl groups due to the lateral projection of the hydrogen atoms in the hydroxyl sites.

Effect of Pore Width. By placing one carbonyl site on each wall, directly opposite each other and varying the pore width (Figure 8a), we can examine the influence of the separation of sites on opposing pore walls.

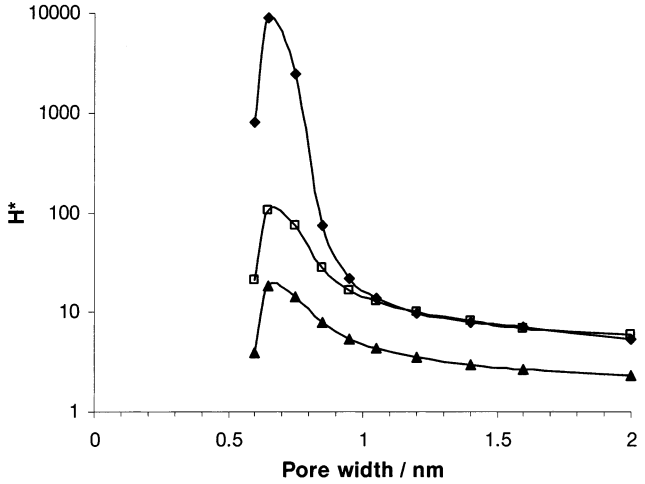

Figure 9. Henry's constant as a function of pore width for carbonyl surface groups. Triangles are for a purely graphitic pore, open squares are for a pore containing two carbonyl groups at maximum lateral separation, and diamonds are for a pore containing two sites directly above each other. Lines are a guide to the eye.

The values of H vs pore width for this case are plotted as diamonds in Figure 9.

The open squares represent an analogous situation, but with the sites at a maximum separation in the x direction (Figure 8b) (in this configuration, they are considered to behave as isolated sites). Also plotted is the change in H with pore width for a purely graphitic pore (triangles).

By looking at the curve for pure graphite we can see that the maximum affinity for adsorption occurs for a pore width of around 0.65 nm. At this width, the attractive potentials of both walls overlap substantially and the potential energy is at its deepest. If the pore width decreases below this value, the repulsive part of the wall potential is predominant and the adsorption is significantly reduced.

The presence of two isolated polar sites significantly increases the Henry's constant relative to graphite, but this increase is virtually independent of pore width (the curve merely shifts to higher values by a constant amount). However, if the sites are directly above each other, this enhancement of adsorption is much higher in small pores. As with two sites on the same wall, this is due to the possibility of a water molecule bonding to both sites simultaneously, across the pore (Figure 10).

When the pore width exceeds 1 nm both curves overlap, indicating that the z separation is sufficient to virtually eliminate cooperation between the two sites that are directly above each other. In this situation, water bonds to only one of the sites and the affinity for water adsorption is independent of their relative position.

A similar study was performed with hydroxyl groups, and the results are shown in Figure 11.

The conclusions we can take are as for the carbonyl surface groups: the pore width above which the relative position of the sites does not affect H is also around 1 nm. This is because the projection of the OH bond in the z direction is very small.

Effect of Local vs Total Site Density. The results from the previous sections show that polar surface sites located in close vicinity to each other behave differently from when they are isolated. To further separate the effects of local from total density of sites, we have examined several more complex configurations involving carbonyl groups. In these configurations we have considered two different categories of sites: closely located sites, separated

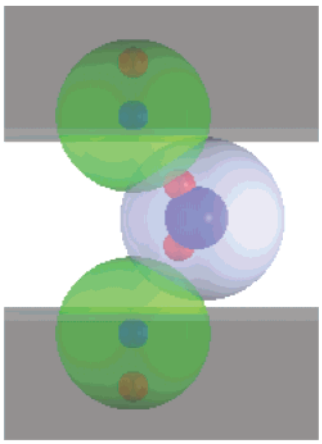

Figure 10. Snapshot of water adsorbing in a slit pore of width 0.75 nm containing carbonyl groups on opposing pore walls. Color coding is the same as in Figure 5.

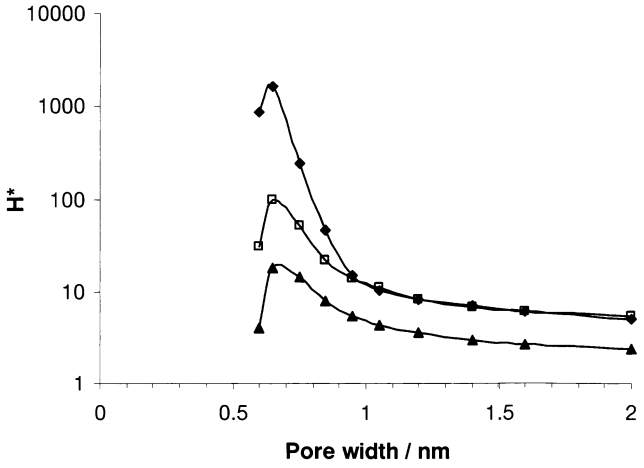

Figure 11. Henry's constant as a function of pore width for hydroxyl surface groups. Triangles are for a purely graphitic pore, open squares are for a pore containing two surface sites at maximum lateral separation, and diamonds are for a pore containing two sites directly above each other. Lines are a guide to the eye.

by 0.3 nm (which we will term "pairs" from now on), and simple isolated sites, separated by at least 0.7 nm.

The first of these case studies involved calculating Henry's constant in a series of configurations starting from a graphitic pore. Subsequent configurations were generated by adding two carbonyl sites at a time, either in pairs or isolated. The results are plotted in Figure 12, from where we can see that the increase in the surface site density causes an increase in the hydrophilicity of the pore. However, this increase is much more pronounced when the sites are paired than when they are isolated. Indeed, the inclusion of a single pair of carbonyl sites on the surface has a stronger effect than the addition of 12 isolated sites.

To further investigate this effect, we have calculated H in a series of pores in which the overall concentration of sites was kept constant, but the number of paired sites was allowed to vary. We now start from a pore with only isolated sites and generate subsequent configurations by moving them one by one into close proximity (Figure 13).

By examining the plot in Figure 14, we can observe a gradual enhancement of the hydrophilic behavior as the number of pairs increases.

We now proceed to examine the influence of these factors at higher pressures. For that purpose, we have calculated

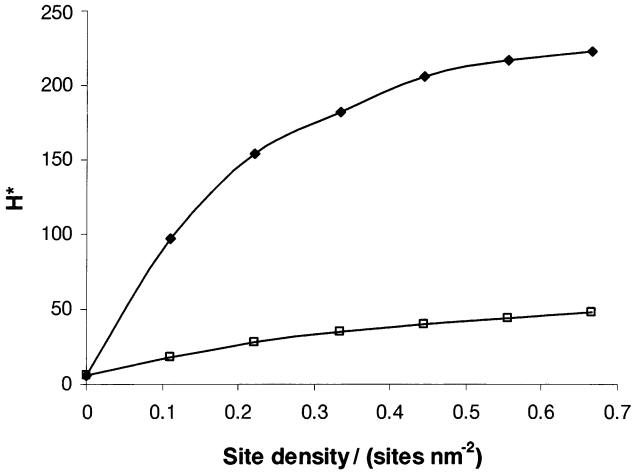

Figure 12. Henry's constant as a function of site density for two different configurations of carbonyl sites. The density is increased gradually by adding pairs (diamonds) or isolated sites (open squares). The pore width is 0.95 nm. Lines are a guide to the eye.

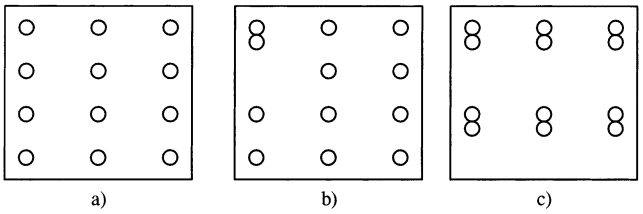

Figure 13. Configurations for the study of local density of carbonyl sites: (a) no pairs; (b) one pair; (c) six pairs. The overall site concentration is the same in all configurations.

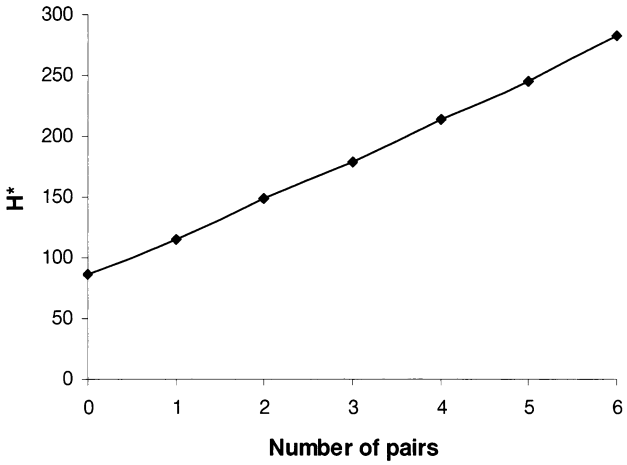

Figure 14. Henry's constant as a function of the number of pairs of carbonyl sites. The pore width is 0.95 nm and the total site density is kept constant at 1.33 nm^{-2}. The line is a guide to the eye.

GCMC adsorption isotherms up to 3000 Pa for different site configurations and concentrations. The first results are for cases analogous to Figure 13, i.e., keeping the overall density constant but changing the number of paired sites. The isotherms for three of those cases are shown in Figure 15.

This type of isotherm is typical of systems characterized by low solid−fluid dispersion interactions but high fluid−fluid affinity.[14] At low pressure, there is hardly any water adsorbed in the pore, but once the pressure is high enough, the fluid inside the pore spontaneously jumps from this low-density vaporlike state to a high-density liquidlike state. In the low-pressure region, the isotherms are linear,

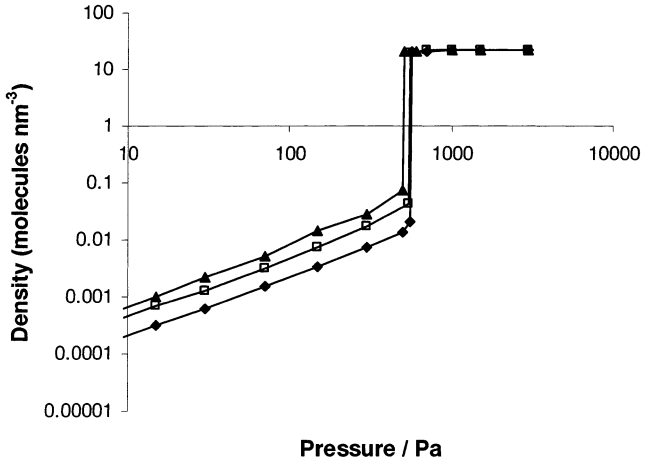

Figure 15. Adsorption isotherms from GCMC simulations in a slit pore of width 0.95 nm with a total density of carbonyl sites of 1.33 nm^{-2}. The number of pairs of sites is 0 for diamonds, 3 for open squares, and 6 for triangles. Data are shown on a logarithmic scale to aid visualization of the isotherms over the entire pressure range. Error bars are the size of the symbols used. Lines are a guide to the eye.

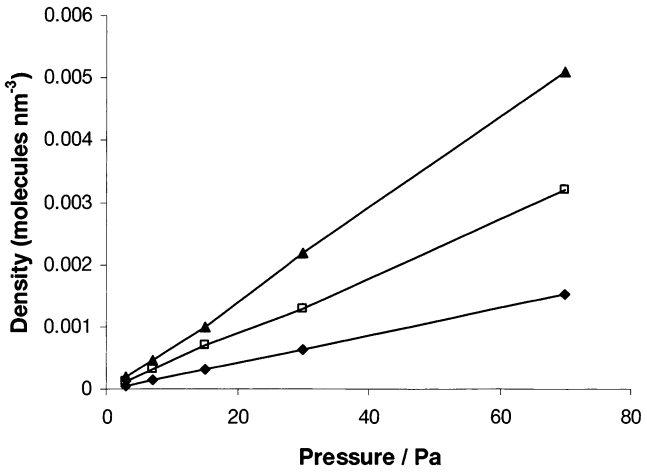

Figure 16. Adsorption isotherms at low pressure from GCMC simulations in a slit pore of width 0.95 nm with a total density of carbonyl sites of 1.33 nm^{-2}. Symbols are the same as in Figure 15.

in accordance with Henry's Law (Figure 16). By comparing the isotherms for different site distributions we can see that the increase in low-pressure adsorption with the number of pairs is once again evident. However, the spontaneous condensation occurs almost at the same pressure for all three configurations (Figure 15), which suggests that it is virtually independent of local site density.

The point at which the spontaneous condensation takes place in a GCMC simulation does not correspond to the true equilibrium phase transition. Rather, it occurs somewhere between the equilibrium and the limit of stability of the vapor phase.[34,39] To verify if the pressure at the equilibrium phase transition is also independent of the local distribution of active sites, we have performed simulations using the gauge-cell method. In Figure 17 we show the results obtained for a pore of 0.95 nm with evenly distributed sites.

Using this method we were indeed able to trace the entire van der Waals loop of the system, as well as to calculate the equilibrium transition pressure. The shape of the loop is qualitatively similar to that of water in purely graphitic pores,[34] with a large extent of vapor metastability. As expected, the point of spontaneous condensation in the GCMC isotherm occurs between the equilibrium value and the vapor spinodal point. The gauge-cell results overlap with the GCMC isotherm in the stable and metastable regions, indicating consistency between both methods. The van der Waals loops obtained for configurations with different local distributions of sites (analogous to Figure 15) differed only slightly from the results shown in Figure 17, so they are not shown here. The only significant difference was observed in the low-pressure region, but this exerted negligible influence on the calculated value of the equilibrium transition pressure. Therefore, we can say that the equilibrium phase transition pressure is virtually independent of the local distribution of surface sites, as long as the total site density remains constant.

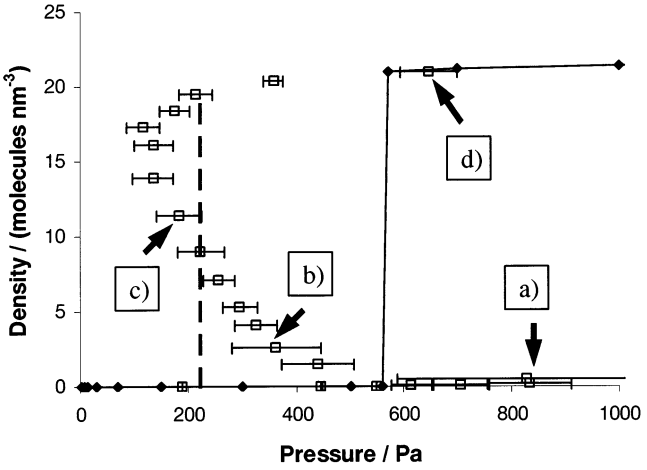

Figure 17. Isotherm for water adsorbed in an activated carbon pore of width 0.95 nm, with a total density of carbonyl sites of 1.33 sites nm^{-2}. The sites are evenly distributed on the surface of the pore (no sites are paired). Filled diamonds are the results of GCMC adsorption, while open squares show the results of the gauge-cell simulations. The pressure at the equilibrium phase transition, calculated by Maxwell's rule, is marked by the dashed line. Error bars in GCMC results are the size of the symbols used. The small arrows and the labels mark the points at which snapshot configurations were obtained.

We have also calculated isotherms in 0.95-nm-wide pores with different values of overall site density, in which the sites were regularly distributed on both walls with separation distances of at least 0.7 nm. The GCMC adsorption isotherms are plotted in Figure 18.

In this case, the adsorption at low pressure is almost independent of site concentration (it is slightly smaller for 0.44 sites nm^{-2} but practically the same for all other site densities). However, spontaneous condensation occurs at very different pressure values. The vapor−liquid equilibrium results for this case study (Figure 19) show the same trend—an increase in the site concentration shifts the equilibrium transition to lower pressures.

By examining the low-density region of the van der Waals loop, we see that as the density of active sites increases, the vapor spinodal point occurs earlier. The presence of more nucleation sites on the surface of the carbon has the effect of reducing the stability of the vapor phase, thus shifting its limit of stability to lower pressures. For the metastable liquid phase, the effect of surface site density is not nearly as significant, presumably due to the dominance of the large number of water−water interactions over the water−solid interactions in the liquid phase. Nevertheless, the presence of surface groups participating in hydrogen bonding does stabilize the liquid phase to an extent.

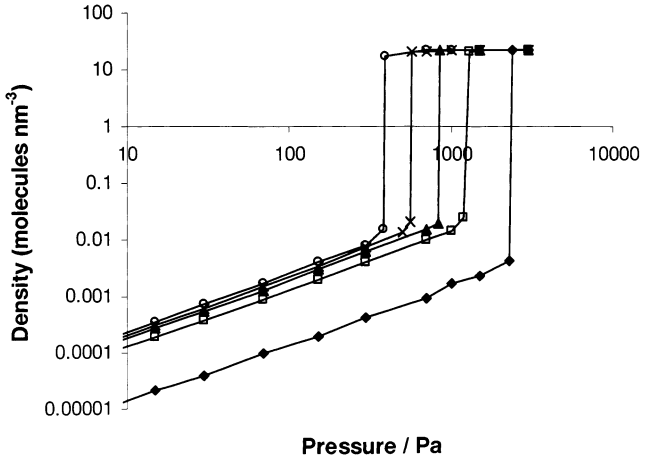

Figure 18. GCMC adsorption isotherms in a slit pore of width 0.95 nm, activated with regularly distributed carbonyl groups. Diamonds are for pure graphite, open squares are for a site density of 0.44 nm^{-2}, triangles are for 0.89 nm^{-2}, crosses are for 1.33 nm^{-2}, and open circles are for 2.22 nm^{-2}.

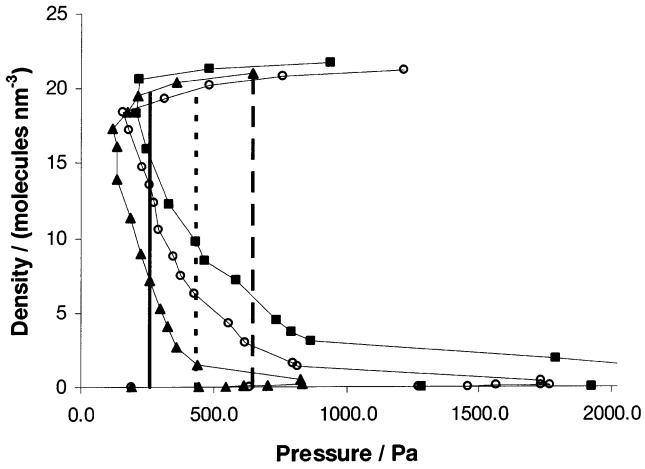

Figure 19. Simulations of vapor−liquid coexistence for water adsorbed in a slit pore of width 0.95 nm, activated with regularly distributed carbonyl groups. Symbols represent the results of the gauge-cell simulations and vertical lines show the values for the equilibrium transition pressure obtained by Maxwell's rule. Filled squares and dashed line are for pure graphite; open circles and dotted line are for a site density of 0.44 sites nm^{-2}; filled triangles and continuous line are for 1.33 sites nm^{-2}. Thin lines connecting the symbols are a guide to the eye. Error bars are omitted for clarity.

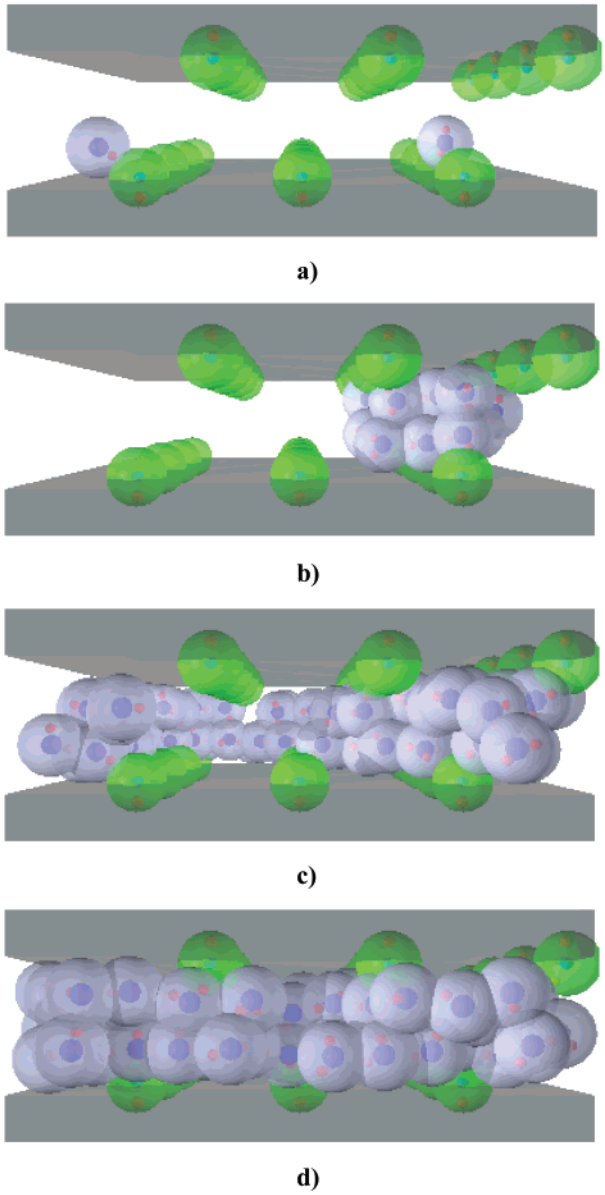

Figure 20. Snapshots of typical configurations for several densities of adsorbed water, corresponding to the points marked by arrows in Figure 17: (a) 0.234 molecules nm^{-3}; (b) 2.34 molecules nm^{-3}; (c) 11.11 molecules nm^{-3}; (d) 21.05 molecules nm^{-3}. Color coding is the same as in Figure 5.

Our results can be better understood by considering the mechanism of condensation of water in slit pores. This is more easily explained with the help of snapshots of typical configurations for several densities of adsorbed water in a pore of width 0.95 nm (Figure 20).

Initially, the pore contains very little adsorbed water, which is mostly bonded to surface sites (Figure 20a). As the pressure increases, density fluctuations in the pore become larger, and short-lived water clusters are seen to occasionally form and disintegrate during the course of the simulation. At a certain point, a cluster that spans the whole of the pore width, connecting both walls, is formed (Figure 20b). Once such a cluster is formed, it is very easy for more water molecules to bond to the existing ones, expanding the cluster laterally along the pore (Figure 20c). After that, the pore quickly fills with a liquidlike phase (Figure 20d). The formation of a pore-spanning cluster seems to be critical to the onset of condensation. It must be noted, however, that configurations b and c in Figure 20 are unstable and do not correspond to points on the equilibrium isotherm. Rather, they are merely observed as intermediate steps in the formation of the liquid phase. This mechanism is similar to that observed for water adsorption in graphite pores but radically different from the condensation mechanism of strongly adsorbing, nonpolar substrates.[34] In light of this mechanism, it is easy to see that if the density of surface sites increases, so does the probability of formation of the pore-spanning cluster. Therefore, condensation occurs at lower pressures in pores with more active sites. The distribution of these sites on each pore wall, on the other hand, has little impact on the probability of formation of such a cluster. Although it strongly affects the amount of water adsorbed at low pressures, the local site density has a small effect on the condensation process.

In relatively narrow pores, such as the 0.95-nm pore, the presence of active sites on opposite walls, as well as the distance between them, is expected to have an influence on the condensation pressure. In Figure 21 we present GCMC water adsorption isotherms in a 0.95-nm

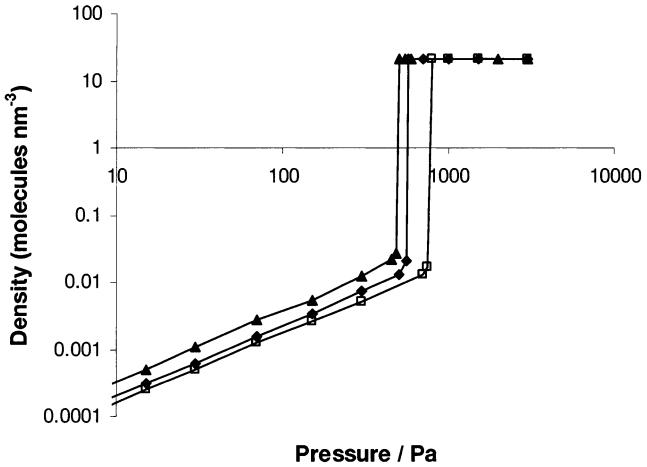

Figure 21. GCMC adsorption isotherms in a slit pore of width 0.95 nm with a total density of carbonyl groups of 1.33 sites nm^{-2} for analysis of the separation between sites on opposite walls. Filled triangles are for sites on both walls, directly opposite each other (relative distance across the pore of 0.7 nm). Filled diamonds are for sites on both walls, at maximum possible separation (0.94 nm). Open squares are for all sites on the same wall.

pore with 1.33 sites nm^{-2}, for three different cases in which we analyze the influence of this factor.

This comparison is analogous to the study depicted in Figure 8, except that we have not varied the pore width. By examining the isotherms, we can see that the relative distance between sites on opposing walls changes not only the low-pressure adsorption but also the point of spontaneous condensation. In the case where the active sites are directly opposite each other, condensation occurs at lower pressures, since the probability of formation of pore-spanning clusters increases. Although we have not performed the same analysis for other pore widths, we expect this effect to be stronger in narrower pores and to be practically negligible in wide pores, in tune with the effect on Henry's constant (see Figure 9). We also show in Figure 21 the isotherm for a configuration where all the sites are on the same wall. If we compare this with the results for maximum site separation, we see that adsorption at low pressure is hardly affected, since the sites are essentially isolated in both configurations. However, spontaneous condensation occurs at higher pressures when all the sites are on one wall, regardless of the fact that it is easier for water molecules to form bridges between surface sites on the same wall in this configuration. Once more, this has to do with the probability of formation of a pore-spanning cluster—it is easier to form such a cluster when there are nucleation sites on both walls. This provides further evidence that it is the formation of a cluster connecting both pore walls that is critical for the onset of the liquid phase, rather than the growth of clusters on the same wall.

To complete this discussion, we have simulated adsorption in pores with different random configurations of carbonyl groups (Figure 22).

The corresponding GCMC isotherms are depicted in Figure 23. In general, low-pressure adsorption increases with the site density, while spontaneous condensation occurs at lower pressures as the number of sites increases.

The exceptions to this rule are the two highest densities—in fact, low-pressure adsorption is higher at a density of 1.78 sites nm^{-2} than at 2.67 sites nm^{-2}. This observation might seem unusual, but we can explain it as follows. In the configuration at 1.78 sites nm^{-2}, a large

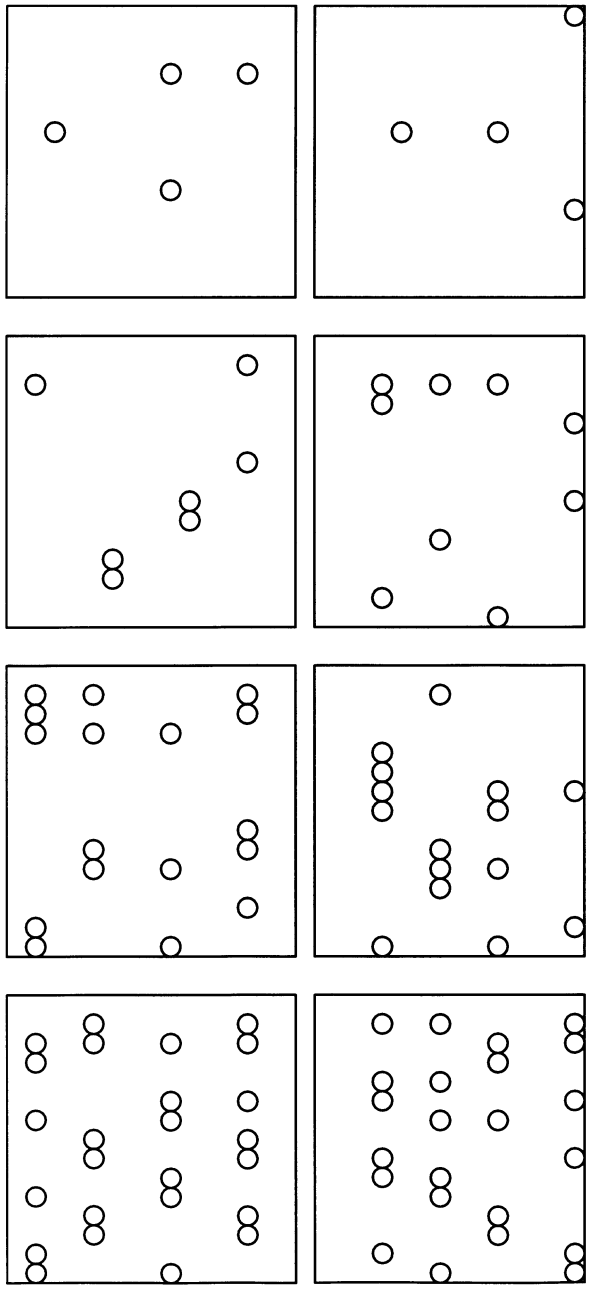

Figure 22. Random configurations of surface sites for values of the total site density, from top to bottom: 0.44, 0.89, 1.78, and 2.67 nm^{-2}. In each case, the left and right boxes represent the two opposing pore walls.

number of carbonyl groups are located in very close vicinity, forming very strong loci for water adsorption, whereas the sites in the highest density configuration are much more regularly distributed (see Figure 22). Therefore, since adsorption at low pressure is mainly determined by local site distribution, we can expect it to be higher in the first case, even if the total site density is lower. As the pressure increases the curves eventually cross over, spontaneous condensation occurring earlier for the higher total density. This provides further evidence for our reasoning that the local distribution of active sites affects mainly low-pressure adsorption, while the total site density is the most important factor in determining the pressure of spontaneous condensation.

Effect of Type of Surface Group. To compare the effects of each type of polar group, we have calculated *H* for different densities of isolated carbonyl, hydroxyl, and

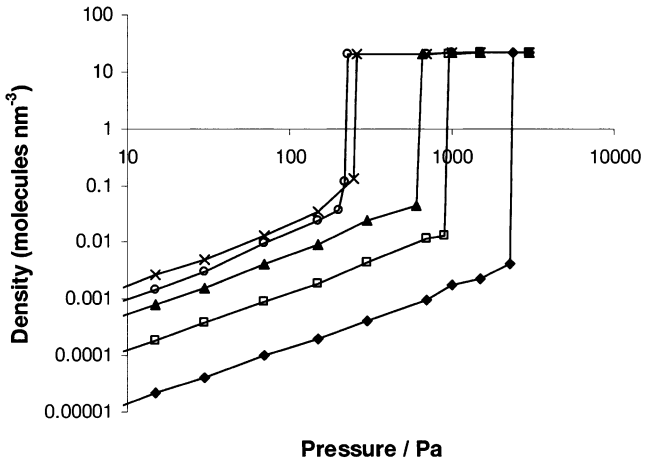

Figure 23. Adsorption isotherms in a slit pore of width 0.95 nm with random distributions of carbonyl sites, corresponding to Figure 22, at different densities: 0.0 nm^{-2} (diamonds), 0.44 nm^{-2} (open squares), 0.89 nm^{-2} (triangles), 1.78 nm^{-2} (crosses), and 2.67 nm^{-2} (open circles).

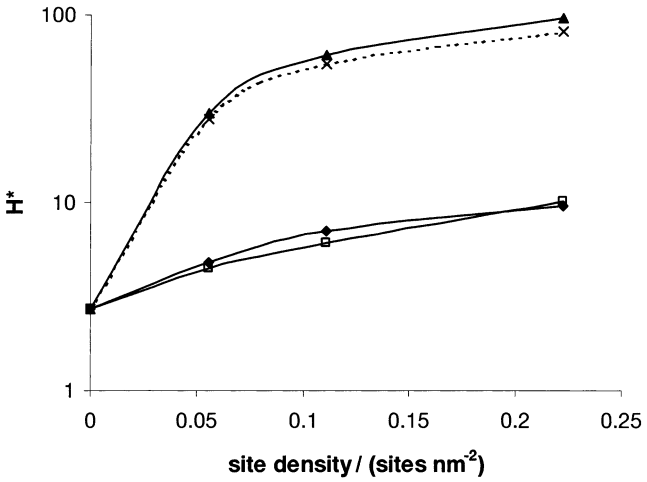

Figure 24. Henry's constant as a function of site density for several types of functional groups: carbonyl (diamonds), hydroxyl (open squares), carboxyl (triangles), and pairs of carbonyl groups (crosses−dotted line). The pore width is 1.6 nm.

carboxyl sites. From the results (continuous lines in Figure 24), we can see that the magnitude of the Henry's constant for isolated carbonyl and hydroxyl groups is similar, but it is much higher for carboxyl groups.

This is mainly due to the fact that a water molecule can form two hydrogen bonds with a single carboxyl group, in a very energetically favorable configuration (Figure 25), while it cannot do so with the other groups.

This observation suggests that one COOH group is essentially behaving as two oxygenated sites placed in close vicinity to each other. In fact, this behavior can be effectively reproduced if we substitute each COOH site by a pair of O sites separated by 0.3 nm (dotted line in Figure 24). Our results are in line with the interpretation of Barton et al.,[17] who have suggested that the amount of water adsorbed in an activated carbon depends only on the density of oxygen on the surface, regardless of its functionality.

The fact that the energy of adsorption of water onto carbonyl and hydroxyl sites is very similar does not mean that the behavior of these sites is exactly the same. In fact, in the case of a carbonyl group the hydrogen bond will always be between its oxygen atom and the hydrogen

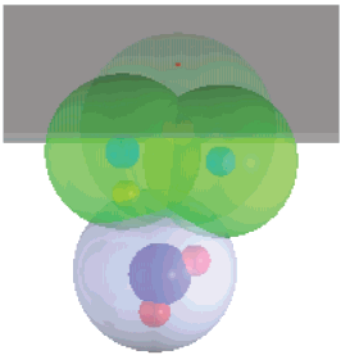

Figure 25. Snapshot of water adsorption in a slit pore of width 0.95 nm with one carboxyl group. Notation is the same as in Figure 5.

in the water molecule, while a hydroxyl group may bind with water using either its oxygen or its hydrogen atom. This will have implications on the structure of the adsorbed water, but the energy of the hydrogen bond will be roughly the same. Similarly, we cannot expect water to be adsorbed in a similar configuration in the presence of a carboxyl group or of two paired carbonyl groups. However, the energy of adsorption will be roughly the same and there will be little impact on the amount adsorbed. Therefore, it is likely that the behavior of a real activated carbon (which contains several different types of polar sites) can be effectively modeled by a distribution of a single type of active site. Carbonyl groups seem the most likely candidates for inclusion in such a model, since they can be represented by a very simple molecular model, which makes the simulations computationally less expensive, and are not orientation dependent. Furthermore, there is experimental evidence of the presence of carbonyl groups on the surface of activated carbons, both isolated and in pairs.[8]

Conclusions

In this paper we have presented a detailed and systematic analysis of the effect of polar surface sites on water adsorption in activated carbon. We have used realistic molecular models and molecular simulation techniques to selectively examine the impact of type, amount, and distribution of polar surface sites on low-pressure adsorption and capillary condensation of water in slit-shaped carbon pores. This study forms a basis for the development of a model that is able to describe both structural and chemical heterogeneity of real activated carbon.

We have shown that adsorption at low pressures is mainly dictated by the local distribution of hydrophilic sites, while capillary condensation depends mainly on the overall density. Furthermore, we have observed that in narrow pores (i.e., below approximately 1 nm), both low-pressure adsorption and capillary condensation depend on the relative distance between active sites located on opposite walls. These findings were explained on the basis of the mechanism of condensation of water in pores, for which the formation of a pore-spanning cluster is critical. This mechanism of condensation seems to be the same in both activated and purely graphitic pores. However, the presence of active sites facilitates the formation of a water cluster connecting both pore walls and thus shifts the condensation pressure to lower values.

From our analysis of several types of oxygenated surface groups, we can conclude that the amount of water adsorbed is mainly affected by the number of oxygen atoms on the surface, rather than by their functionality. Therefore, more

complex sites can be thought of as combinations of simpler sites without prejudice to the adsorbed amount.

In the development of a model for activated carbon, all these factors must be taken into consideration. In particular, one must proceed with caution when trying to represent the chemical heterogeneity of activated carbon by using a random distribution of surface sites (such an attempt has been made, for example, by McCallum et al.[25]). Such a distribution might have an uncharacteristically high affinity toward water, in which case the model carbon will tend to adsorb more than the real carbon (or vice-versa). To model the behavior of a real carbon by using random distributions of surface sites, one would have to calculate a statistical average over a significant number of possible site configurations. Such a large number of simulations would be very computationally demanding. A more practical model would be obtained by generating a "representative" configuration that takes into account all the important characteristics that affect water adsorption. For instance, the distribution of pore widths could be obtained by analyzing experimental adsorption isotherms of nonpolar species.[3] With this information, one could in principle introduce active sites in the pores, by using an effective site model (e.g., carbonyl groups). The overall concentration of these sites could be obtained from the high-pressure region of the experimental water adsorption isotherm, while the low-pressure region would provide information about their distribution on the pore walls.

Acknowledgment. M. Jorge acknowledges financial support from Fundação para a Ciência e Tecnologia—Programa PRAXIS XXI.

LA025846Q